

Thin corrugated-edge shells inspired by Nervi's dome: numerical insight about their mechanical behaviour

M. Lai[a,*], M. Zucca[a], D. Meloni[a], E. Reccia[a], A. M. Cazzani[a]

[a] *Dipartimento di Ingegneria Civile Ambientale e Architettura, Università degli Studi di Cagliari, Cagliari, Italy*

Abstract

During last decades, the constant evolution of the construction systems has led to the possibility of carrying out increasingly complex architectural project. Among the wide range of construction systems, concrete thin corrugated-edge shells stand out for their relevance. In this paper, the mechanical behaviour of thin concrete corrugated-edge shell inspired by Nervi's Flaminio dome has been analysed in detail, considering different load configurations (self-weight, uniform vertical pressure and antisymmetric vertical load) and constrains (pure membrane and displacements restrained boundary conditions). Non-linear static analysis has been performed to assess the vertical load-bearing capacity of the corrugated-edge shell considering Concrete Damaged Plasticity (CDP) constitutive model and linear and non-linear buckling analyses have been carried out to evaluate the effects of the corrugation on buckling behaviour. The results obtained from linear and non-linear analyses have been compared with those obtained for a concrete thin smooth-edge shell having the same geometric global characteristics. The comparison

*Corresponding author
Email address: `matteolai@unica.it` (M. Lai)

highlighted improvements provided by corrugated-edge in terms of structural behaviour.
Keywords: shells, concrete shells, corrugated dome, domes, Flaminio dome, Pier Luigi Nervi

1. Introduction

Thin concrete shells constitute a paramount illustration of how theory and practice are encountered. The use of concrete shells started at the beginning of the XX century simultaneously with concrete technology development, particularly for special purpose buildings such as gas tanks and thin-walled domes. The theory foundations were laid by numerous scholars in the latest part of XIX century [1], lately by [2]. Between the late 30s and 60s of XX century, shell construction lived its most spreading period, due to the cheap workforce and the use of wood and pneumatic formwork. Usually, they were built for large roofs, silos for powder materials, reservoirs and tanks for liquids, dams, chimneys, and cooling towers. The superior aesthetics and the ability of such structures to span large spaces avoiding intermediate support made this solution a very popular one. Besides, from a Structural Mechanics point of view shell structures are characterized by high strength-to-weight and stiffness-to-weight ratios. In pursuing the most effective shape accounting for both mathematical and mechanical solutions and construction feasibility, the most noteworthy designers were Eduardo Torroja in Spain, Felix Candela in Mexico, Pier Luigi Nervi in Italy and Heinz Isler in Germany. A look into the attitude of that time could be given looking at [3, 4]. Since the 60s shell constructions have declined due to the upsurge of the formwork price for curved surfaces, especially when compared with the development of steel-spatial structures that can solve most of the issues for the long-spanning building in a more cost-effective way.

Attention must be paid to the smoothness condition at the boundary. It is well known that to ensure a pure membrane regime, the constraints must be such that they do not perturb the stress distribution that would occur in an indefinitely extended membrane. To that aim, restraints must act along the meridian direction only. As a consequence, reaction must not have any components in the normal direction to the shell. Other different boundary configurations disturb the membrane state and lead to relevant bending moments concentrated nearby the edge. A well-established analysis tecniques of shell structure in scientific literature relies on the decoupling of membrane and flexural regimes. A simplified analytical solution for the latter problem is provided by [5]; another contribution is given by [6]. From a practical point of view the perturbation occurring at the edge is unavoidable: in the field of civil engineering structures, it is difficult to technically realize the constraints needed for a purely membrane regime. Considering that bending effects are restricted to a limited zone near the edge, among the various solutions adopted by designers, there are i) increasing the shell thickness or ii) building a ring beam at the edge. When Nervi found himself involved in the structural design of the Flaminio's dome for the Olympic Game in 1960, the contractors' demands were for a 60-metre roof for a stadium in the Flaminio district in Rome to host boxing matches. The architectural design was commissioned to Annibale Vitellozzi and Nervi was involved in the structural design in order to find an optimized shape for such a large span.

An innovative solution for limiting the bending moment near the edge was proposed; it consisted in increasing the inertia of the shell section nearby the edge adopting a smooth wavy shape without increasing the thickness. Historical pieces of information about the building techniques are elucidated in Nervi's books [7, 8] and [9]. Besides, SIXXI project has given new light to the Italian concrete engineering school, of which Nervi was one of the pre-eminent representatives (see [10]). The evidence of the recent refurbishment undertaken by the Municipality of Rome is reported in [11]. The *Palazzetto Flaminio*, is a sport facility, whose rooftop is a shallow spherical dome made of low-reinforced concrete –patented by Nervi– referred to as *ferrocemento*. It is supported by 36 equally spaced radial pillars, that are inclined to catch the shell slope at the edge and lie on a circular ring foundation. The dome is made by assembling the pre-cast individual pieces at ground level, then they are singularly placed upon a scaffolding. Once all the pieces were in place, a connecting casting was executed. From a qualitative point of view, the corrugation built on the edge of the shell draw to two major structural enhancements:

- firstly, the behaviour improves the membrane regime and reduces the bending effect at the edge. Corrugation provides a stiffness increase without the need of increasing the thickness. A simple model that illustrates the idea behind this option can be found in [3];

- secondly, it is a well established fact that surfaces with free edges are weak and subjected to inextensional deformation, *i.e.* the surface bends without evoking significative strains in the middle surface. A complete mathematical description of this phenomenon is given in [1], while some

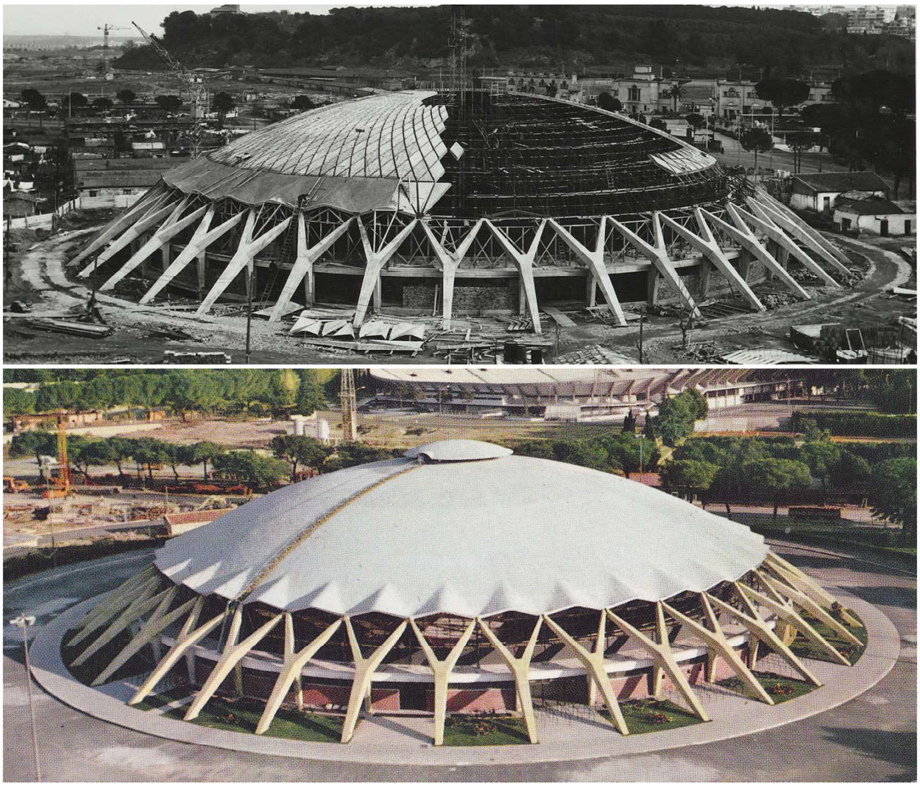

Figure 1: (Above) View of the dome during in-between stages of construction, and of the scaffolding system used to build it. (Below) View of the completed dome.

remarks about it can be found in [12].

A framework of theory of shells is given in [2, 13–15]. A deep study about the behaviour of concrete made shells is reported in [16, 17, 12, 17, 18]. Particular attention about instability phenomena in concrete shells is drawn in [19]. The attention for such aspects are highlighted in the European design recommendations [20]. Finally, a thorough coverage about construction details for concrete shell can be found in [21–23]. [24] reports a parametric analysis concerning the role of corrugation in improving the seismic resistance of vaults and domes, inspired by Eladio Dieste's works of architecture.

Attention to purely compressed shells is highlighted in [25].

This study addresses the effect of boundary conditions on shells behaviour, as it is well-known that different boundary conditions lead to different stress distributions. Besides, the effect of the combination of boundary conditions and different edge geometry is highlighted. Moreover, a detailed analysis is presented for the design of the edge and of the supports, since different restraint conditions may affect the buckling ultimate load. This aspect should carefully be tackled, because such kind of structures are really thin in comparison with the span, and the assessment of the buckling behaviour is an uttermost part of the design process [26]. The correct evaluation of static stresses serves as the backdrop of a buckling analyses, as it has been stressed in [27] and [28] especially with regard to sudden collapse.

Specifically, the case of a wavy-corrugated edge shell is exploited. In Section 2 the geometrical representation of the corrugated edge shell is introduced in such a way that mathematical parametric equations are given. In Section 3 the linear elastic structural behaviour is addressed with respect to three load cases: pressure load, self-weight load and antisymmetric vertical load. Furthermore, two boundary conditions are considered: pure membrane boundary condition and fully restrained displacements. The discussion provides a comparison with a geometrically comparable spherical dome. In Section 4 such a comparison is carried out with regard to the ultimate load bearing capacity in the plastic range. In Section 5 the effects of corrugation on buckling behaviour is evaluated. Finally, Section 6 provides some concluding remarks about the structural improvement of shell edge corrugation.

2. Dome geometry

In this section, a mathematical description of a wavy-edge surface is provided. The shape is inspired by Nervi's Flaminio dome in Rome. Equations for edge-corrugated surface are described in [29]; in the following discussion, a more adherent shape to the original one is presented, where the meridian passing through the support is perfectly spherical. This update allows highlighting the membrane state of the shell. The adopted spherical polar reference system is depicted in Fig. 2, where r is the radial distance from the pole, ϑ is the colatitude angle (the complement to the latitude angle) and φ the longitude angle. Therefore, a point P in a 3-D space is uniquely identified by its spherical coordinates (r, ϑ, φ). A parametric representation of the corrugated-edge spherical surface can be given by introducing a parametrization of its radius. Introducing the equation for a spherical shell, whose radius is R_0, the parametric equations are:

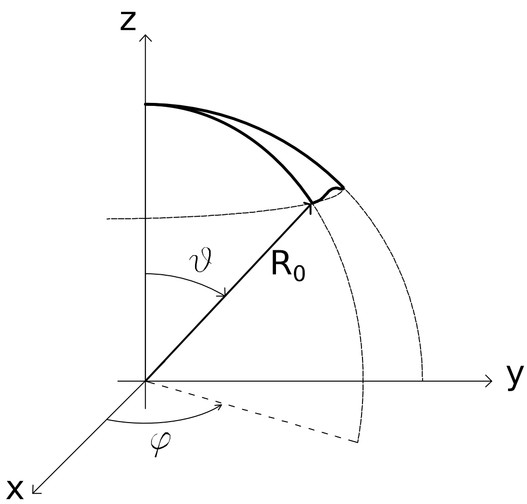

Figure 2: Spherical coordinate system.

$$\begin{cases} x = R_0 \sin\vartheta \cos\varphi \\ y = R_0 \sin\vartheta \sin\varphi & \vartheta \in [0, \pi/2]\,, \varphi \in [0, 2\pi\,)\,. \\ z = R_0 \cos\vartheta. \end{cases} \tag{1}$$

Starting from Eq. (1) by squaring and summing up both sides, parameter ϑ and φ can be eliminated and the resulting *implicit* representation of the spherical surface is obtained:

$$x^2 + y^2 + z^2 - R_0^2 = 0. \tag{2}$$

Now, recalling that the radial distance r is given, in terms of Cartesian coordinate, by

$$r = \sqrt{x^2 + y^2 + z^2}, \tag{3}$$

an *explicit* representation of the spherical surface results: $r = R_0$.

This formulation is used to introduce corrugation on the surface. It is worth noting that in the case of a spherical shell, the radius r is constant and does not depend on the coordinates, whereas in the case of a wavy shape, the radius changes periodically depending on the coordinates ϑ, φ. For such kind of surface, the radius will be $r = r(\vartheta, \varphi)$; besides, one could introduce the corrugation as a perturbation added to the constant radius R_0 of the sphere:

$$r = R_0 \left[1 + f(\vartheta) g(\varphi)\right]. \tag{4}$$

In Eq. 4 the perturbation is composed by two elements: the first one is $f(\vartheta)$ that controls at which colatitude angle the perturbation starts (i.e. the

Table 1: Geometry of Flaminio's Dome in Rome

L_0 span [m]	R_0 radius [m]	f rise [m]	t thickness [cm]
58.5	48.5	5.8	20

opening angle ϑ_0), the second one relies on longitude angle φ and controls the shape of the parallels. In order to get a cyclic symmetry on the surface, function $g(\varphi)$ must be periodic; consequently an appropriate choice to obtain a smooth repetition by a number of waves equal to n is:

$$g(\varphi) = \cos(n\varphi) \tag{5}$$

Function $f(\vartheta)$, which controls the perturbation of the radius along the meridian with reference to that of a perfect sphere, R_0, can be chosen in several ways. A possible choice is:

$$f(\vartheta) = aH(\vartheta - \vartheta_0)\left(\frac{\vartheta - \vartheta_0}{\vartheta_f}\right)^2. \tag{6}$$

Where a is a parameter controlling the amplitude of the perturbation, ϑ_0 is the colatitude angle where the perturbation begins, ϑ_f is the colatitude angle corresponding to the surface edge and $H(\vartheta - \vartheta_0)$ is the Heaviside's step function defined as:

$$H(\vartheta - \vartheta_0) = \begin{cases} 1, & \text{if} \quad \vartheta \geq \vartheta_0 \\ 0, & \text{if} \quad \vartheta < \vartheta_0. \end{cases} \tag{7}$$

The role of $H(\vartheta - \vartheta_0)$ is to switch on the radius perturbation in correspondence of the angle ϑ_0, namely the colatitude angle at which such perturbation originates. Summing up all these ingredients, the following expression for the dome radius is proposed:

$$r = R_0 \left\{ 1 + \frac{a}{2} H(\vartheta - \vartheta_0) \left(\frac{\vartheta - \vartheta_0}{\vartheta_f} \right)^2 [1 - \cos(n\varphi)] \right\}. \tag{8}$$

The main advantage of this formulation is that the amplitude of corrugation at the dome edge can be easily controlled. For the undulated part of the shell, the radius expression is:

$$r = R_0 \left\{ 1 + \frac{a}{2} \left(\frac{\vartheta_f - \vartheta_0}{\vartheta_f} \right)^2 [1 - \cos(n\varphi)] \right\}. \tag{9}$$

So, the function describing the undulated shape of the edge varies between two extrema: for $\varphi = \dfrac{2k\pi}{n}$ $(k \in \mathbb{N})$ one obtains:

$$r_0 = r\left(\varphi = \frac{2k\pi}{n} \right) = R_0, \tag{10}$$

while for $\varphi = \dfrac{(2k+1)\,\pi}{n}$ the result is:

$$r_1 = r\left(\varphi = \frac{(2k+1)\,\pi}{n} \right) = R_0 \left\{ 1 + a \left(\frac{\vartheta_f - \vartheta_0}{\vartheta_f} \right)^2 \right\}. \tag{11}$$

Let h be the maximum amplitude of corrugation at the edge for $\vartheta = \vartheta_f$; then $h = (r_1 - r_0)/2$. To set this amplitude h of the cosine curve to an assigned value, it has to be either:

$$2h = a \left(\frac{\vartheta_f - \vartheta_0}{\vartheta_f} \right)^2 \quad \text{or} \quad a = 2h \left(\frac{\vartheta_f}{\vartheta_f - \vartheta_0} \right)^2. \tag{12}$$

Returning now the example problem, the dimension of the Nervi's dome are listed in Table 1; a comprehensive reference source for the survey of dome dimensions is [30].

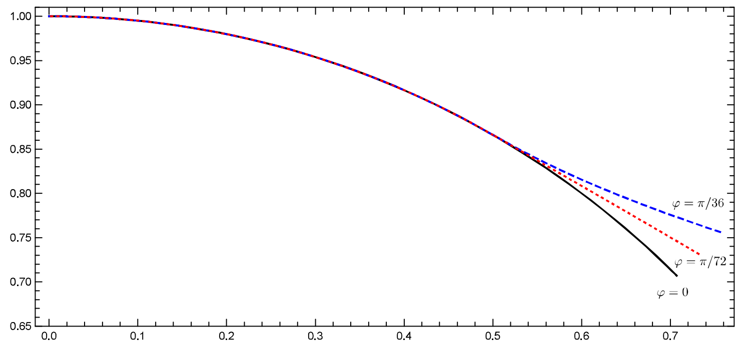

Figure 3: Plot of the cross-sections of the corrugated shell equations with Heaviside's function for three selected values of the longitude angle producing the maximum perturbation (blue dotted curve), zero perturbation (black curve) and intermediate perturbation (red dashed curve). These values of the parameters have been adopted: $R_0 = 1$, $a = 0.6$, $n = 36$, $\vartheta_0 = \frac{\pi}{6}$, $\vartheta_f = \frac{\pi}{5}$. Dimensionless coordinates have been used, by adopting the ratio between the actual values and the radius.

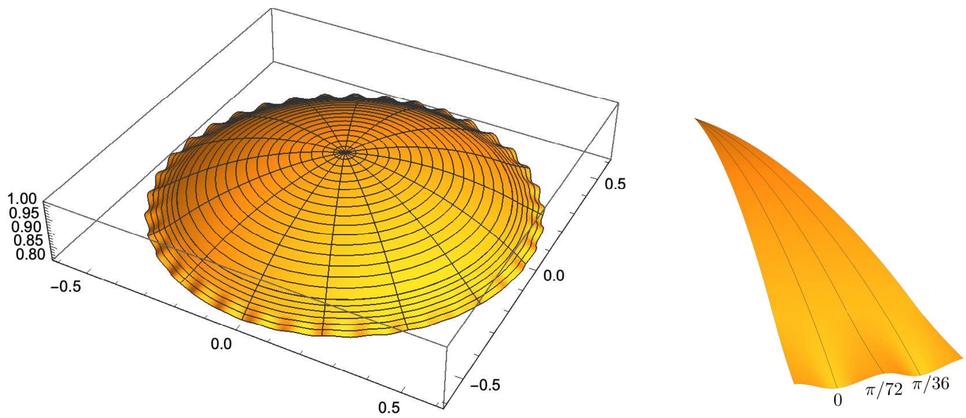

Figure 4: (left) Plot of the corrugated shell surfaces $r(\vartheta, \varphi)$ with Heaviside's function. These values of the parameters have been adopted: $R_0 = 1$, $a = 0.6$, $n = 36$, $\vartheta_0 = \frac{\pi}{6}$, $\vartheta_f = \frac{\pi}{5}$; (right) a magnified part of the dome, where the selected meridians are highlighted.

3. Evaluation of structural behaviour

It has been assumed that the dome is made of C20/25 reinforced concrete. The material behaviour is analysed only with regard to the linear-elastic part of constitutive behaviour, hence, plasticity is disregarded in this Section. Density γ is assumed to be 2500 kg/m^3, Young's modulus is 30 GPa, and Poisson's coefficient is 0.2. Furthermore, for sake of simplicity the RC is always assumed to be uncracked, and time depending effects (*fluage*) are not taken into account. Ref. [31] explains the special construction techniques adopted by Nervi, and their application in some major Nervi's works and how *ferrocemento* made structure can now be refurbished with reference to two buildings.

The investigated dome analyses are carried out with different boundary conditions, namely:

1. pure membrane boundary conditions: supports restrain displacements only along the tangent direction. Rotations are allowed (see Fig. 5 (a)).
2. displacements fully restrained: the displacements along the x, y and z directions are restrained. Rotations are allowed (see Fig. 5 (b)). In this case, flexural effects are not negligible.

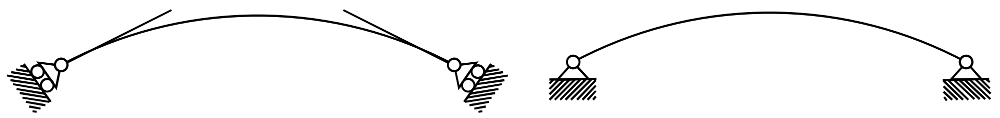

(a) (b)

Figure 5: Adopted boundary conditions: (a) pure membrane; (b) fully restrained displacements.

The constrains are discretely applied on the 36 supports, so the edge between two subsequent supports is free.

Structural behaviour in the two different boundary conditions has been compared considering the two proposed shapes of the dome (the smooth and the corrugated one). Thus, several load-cases (uniform normal pressure, self-weight and antisymmetric vertical load) are addressed in order to compare comprehensively the structural improvement provided by the corrugation at the edge with respect to the smooth shell. The adopted FE model has 30564 8-nodes shell elements.

A simplified structural analysis of Nervi's dome has been already carried out in [32], but without considering edge-corrugation; besides a different opening angle has been assumed in the above-mentioned reference, which, however, does not seem to agree with the architectural blueprints reported in [30].

3.1. Pressure load

The structure is loaded by a uniform external normal pressure q_0 whose magnitude is 5 kPa, applied inwards to the whole surface. Since the extension of the shell is such that its rise to span ratio makes it rather shallow, it is possible to approximate the self-weight load condition with such pressure. This approximation allows tackling the problem of edge-corrugated shells in an easier framework. Nevertheless, it constitutes a significant load-case for pressurized vessels or maritime applications. Let N_φ and N_ϑ be the membrane forces acting in the meridional and parallel directions. The stress σ_ϑ and σ_φ are:

$$\sigma_\vartheta = \frac{N_\vartheta}{t}, \ \ \sigma_\varphi = \frac{N_\varphi}{t}. \tag{13}$$

Where t is the shell thickness, whose value is constant and equal to 0.20 m. The numerical outcome of the analyses are presented in terms of membrane stresses, σ_ϑ and σ_φ. The former represents the stress along the meridian direction and the latter one the hoop stress. All numerical results related to stress are presented in dimensionless form: stress value are divided by the applied external pressure $q_0 = 5$ kN, while the angular position is given in the dimensionless form ϑ/ϑ_f, where ϑ_f is the colatitude value corresponding to the position of the edge, which is assumed to be the same in all considered cases. Fig. 7 shows an example of the reaction forces for both shapes of the shell in pure membrane conditions.

A common drawback occurs when shell stresses are evaluated in a restrained node, because of the chosen discrete boundary conditions at the edge, which produces stress singularities. This issue is well-known in the frame of FE analyses with shell elements [33]. Fig. 8 (left) shows the distri-

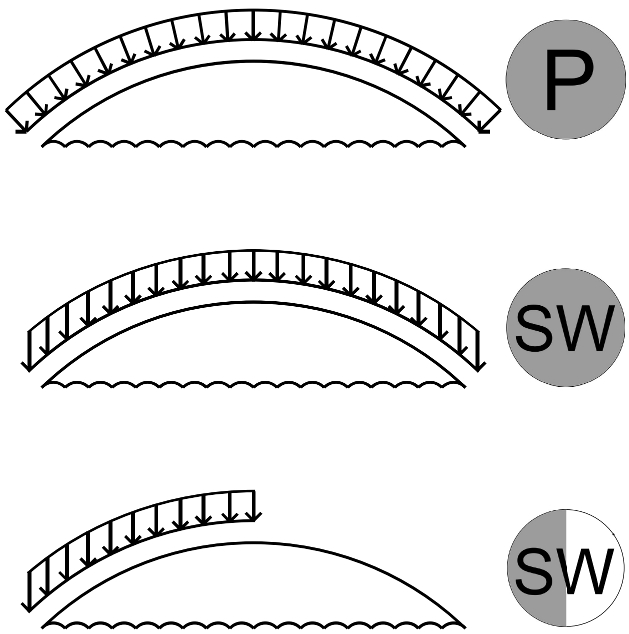

Figure 6: Load cases.

bution of σ_ϑ/q_0 for the analysed four cases. As expected, the behaviour does not depend on boundary conditions if the dimensionless colatitude angle is less than 0.75, and the four curves practically coincide. The aforementioned notation will be used henceforth in all the analysed load-cases. For colatitude values larger than 0.75, the curves for the pure membrane example are not significantly affected by a change of shape, whereas, for the restrained displacement example the corrugated-edge shape presents a significant reduction of the stress in comparison with the smooth shape nearby the edge. Similar considerations can be made for Fig. 8 (right), that shows σ_φ/q_0; here indeed, the effect of stress decreasing due to edge-corrugation is evident in both constrained displacements and pure membrane boundary conditions.

Let M_ϑ be the section moment (which is dimensionally expressed as the ratio moment/thickness, thus being homogeneous to a force) along the ϑ direction and M_φ be the section moment along the φ direction. The output is shown in Fig. 9 in dimensionless form, by dividing the relevant values by a constant M_0 equal to 5000 kN.

Fig. 9 (left) shows M_ϑ/M_0: the pure membrane behaviour is granted until ϑ/ϑ_f reaches the value 0.8, apart from the case of corrugated-edge and restrained displacements boundary conditions, where the behaviour deviates from pure membrane already for values close to 0.6. Beyond these values the flexural effect is not negligible. For both cases the edge-corrugated shape yields a reduction of nearly one-half of the bending moment values at the edge with respect to the smooth shell.

Fig. 9 (right) shows M_φ/M_0; the pure membrane behaviour stands until ϑ/ϑ_f reaches a value of about 0.7; beyond that value the bending effect is relevant. The effect of the shape change at the edge is less relevant than for the case of M_ϑ, as expected for the analysed shape, which is mainly corrugated along the meridian. Nonetheless, there is a clear change in the sign of the bending moments.

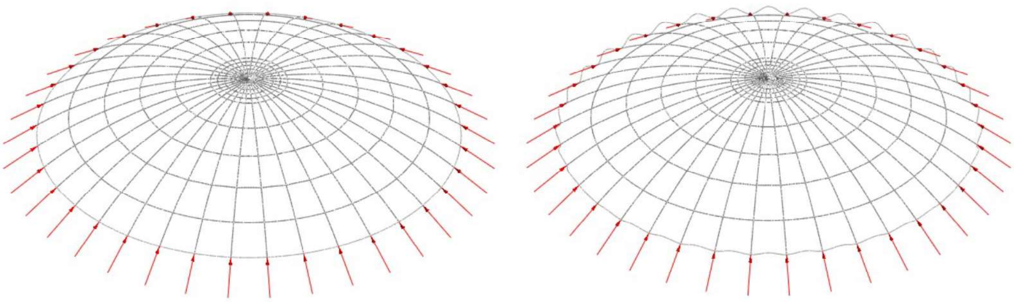

Figure 7: Trust network of the smooth shell (left) and of the corrugated shell (right).

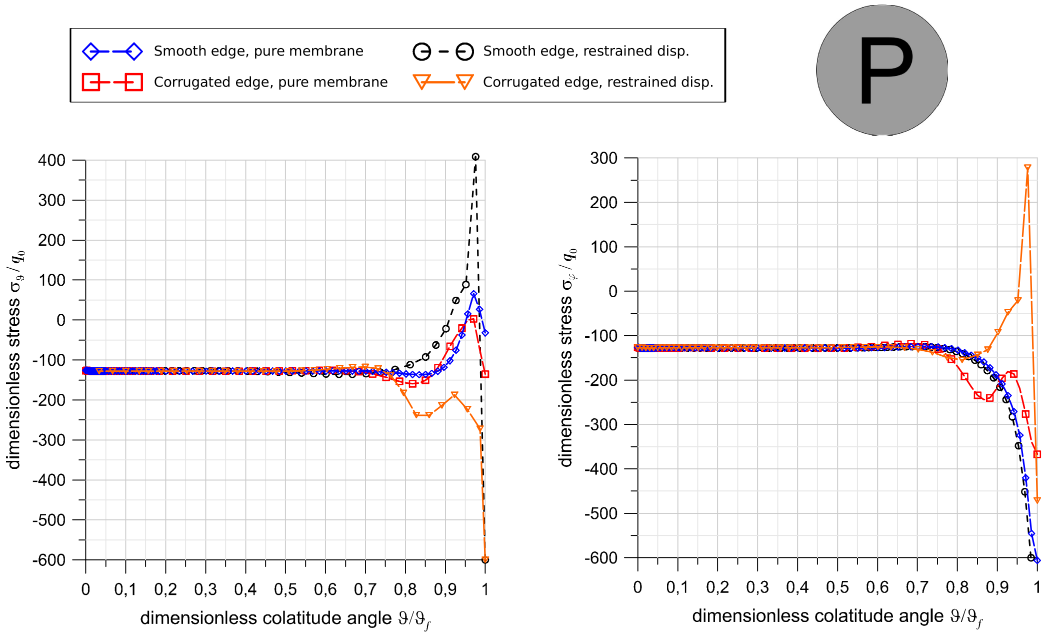

Figure 8: Pressure Load - Stress components σ_ϑ (left) and σ_φ (right) along a meridian passing through a support.

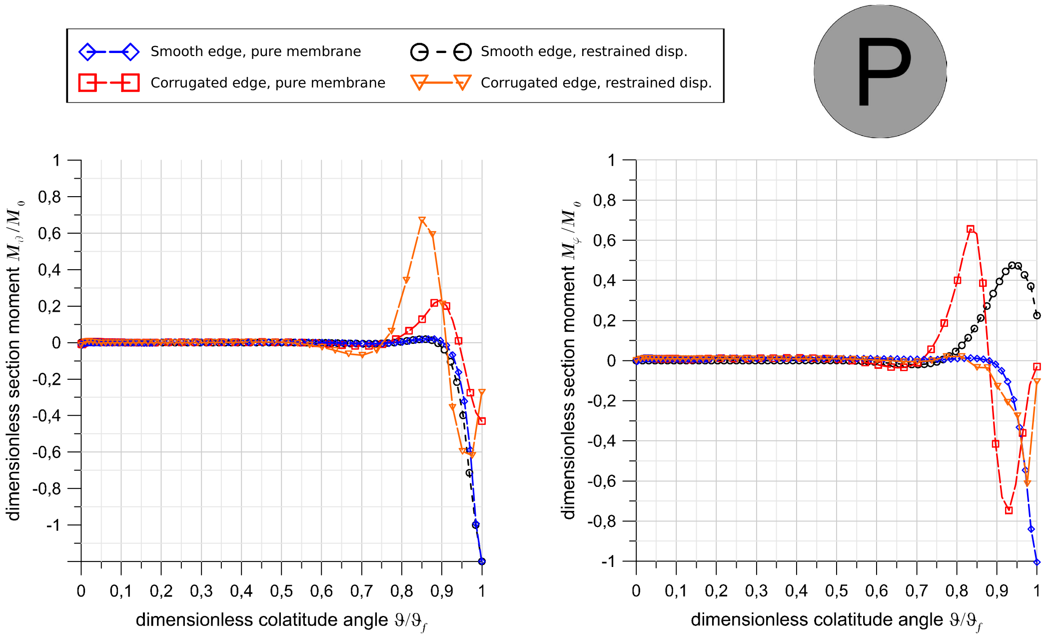

Figure 9: Pressure Load - Section moments M_ϑ (left) and M_φ (right) along a meridian passing through a support.

3.2. *Self-weight load*

The most relevant load-case for concrete domes is the self-weight load, hereby computed using the standard practice and design density value. Fig. 10 shows the distribution of σ_ϑ/q_0 for the analysed four cases. Again, the behaviour does not depend on the boundary condition if the dimensionless colatitude angle is less than 0.75. Beyond such value, no advantages are provided by corrugation of the edge, both in the case of pure membrane and restrained displacements boundary conditions.

The corrugated-edge shell stress curve outlines an inversion from compressive to tensile values close to the edge, but vanishes in correspondence to the edge. On the contrary, for such effect the restrained displacements case the stress is always on compressive, even on the nearby support. Different considerations can be made for Fig. 10 (right), that shows σ_φ/q_0; the membrane state here is reliable until ϑ/ϑ_f reaches 0.6; indeed, the edge-corrugation does not improve significantly the hoop stresses, it rather worsens the stress concentration in the case of restrained displacements boundary condition. Fig. 11 (left) shows M_ϑ/M_0; the pure membrane behaviour stands until ϑ/ϑ_f reaches the value 0.6. From that point on significant bending moments occur. While for the pure membrane boundary condition the edge-corrugation does not provide remarkable improvements, in the restrained displacements case there is a noteworthy reduction of the bending moment values at the edge with respect to the smooth shell. Fig. 11 (right) shows M_φ/M_0; the pure membrane behaviour is confirmed until ϑ/ϑ_f reaches the value 0.7. As previously stated in Sec. 3.1, and as expected, the effect of a shape change at the edge is less relevant than for the case of M_ϑ, apart from the case of pure membrane boundary condition.

3.3. Antisymmetric load

It is of interest in practical design to carry out extensive analyses of domes subjected to non symmetrical loads: for instance, wind load and special combination involving snow load should be carefully considered. The structure will be now analysed under an antisymmetric vertical load, *i.e.* a distributed load applied only on a semi-cap, whose magnitude is 5kN/m^2 (see Fig. 6). Due to the lack of symmetry of the problem, results will be shown along three different meridians, named A, B, and C corresponding to longitude angles φ equal to respectively of $\pi/2$, $3/4\pi$, and π, (see Fig. 12) this time considering that angular coordinate ϑ takes values between $-\vartheta_f$ and ϑ_f, al-

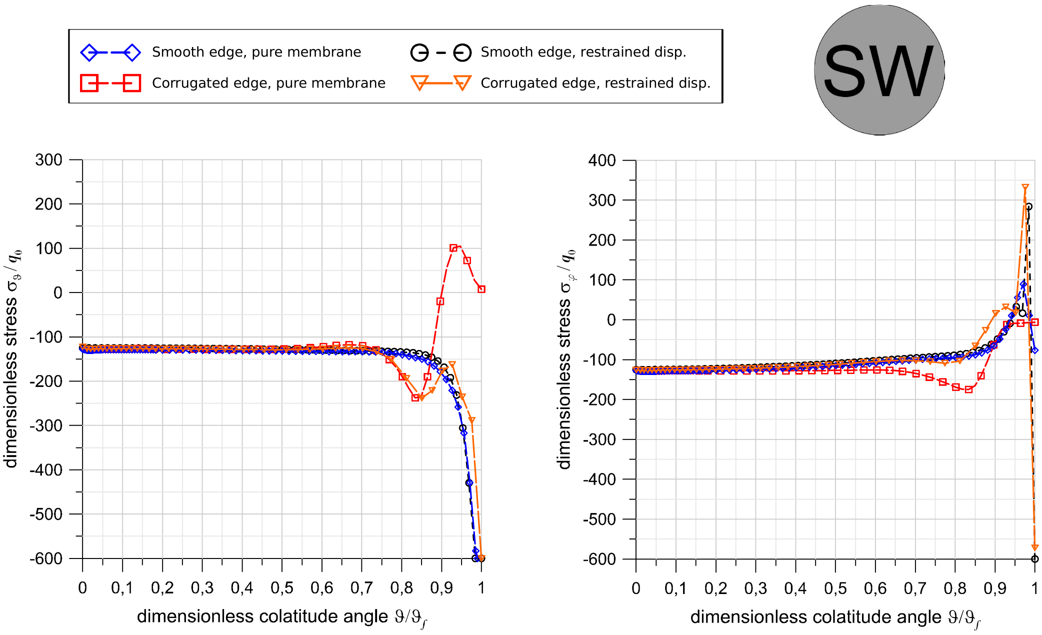

Figure 10: Self-weight Load - Stress components σ_ϑ (left) and σ_φ (right) along a meridian passing through a support.

lowing the effect of the load to be read in both the loaded and unloaded parts. The same figure also depicts the loaded portion of the shell. Thence, meridian A is symmetrically loaded for the whole length, meridian B is loaded only in the second quadrant and meridian C is loaded anti-symmetrically. Fig. 13 (left) shows the membrane stress σ_ϑ for meridian A, whose behaviour is as expected perfectly symmetrical. The behaviour does not depend on the boundary condition for dimensionless colatitude within ± 0.8 and the four curves practically coincides. Beyond ± 0.8, only the curve for the restrained displacements condition in the corrugated-edge shell, the stress remains compressive, whereas the other three curves show tensile stresses near the edge, with possible crack issues if no tension material were considered.

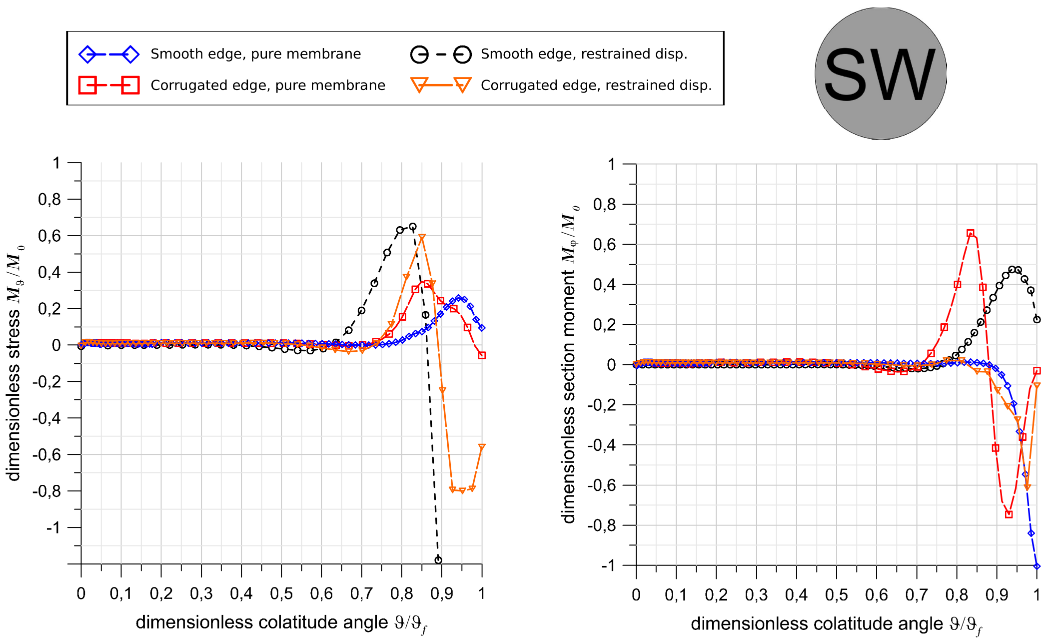

Figure 11: Self-weight Load - Section moments M_ϑ (left) and M_φ (right) along a meridian passing through a support.

Fig. 13 (right) shows the membrane stress σ_φ for meridian A. The perfectly symmetrical behaviour, is independent from the shape of the shell and from its boundary conditions and follows a pure membrane regime within the values of dimensionless colatitude angle equal to ± 0.8. Beyond ± 0.8, only the curve for restrained displacements condition and corrugated edge shell shows, this time, a relevant tensile stress nearby the constrains.

Fig. 14 (left) shows the membrane stress σ_ϑ for meridian B. The effect of the load is noticeable for ϑ/ϑ_f between 0 and 1 and particularly intense on the edge; on the other half it is practically irrelevant except near the constraint, where some minor stress peaks are detected. Fig. 14 (right) shows the membrane stress σ_φ for meridian B. The effects due to the load are the same

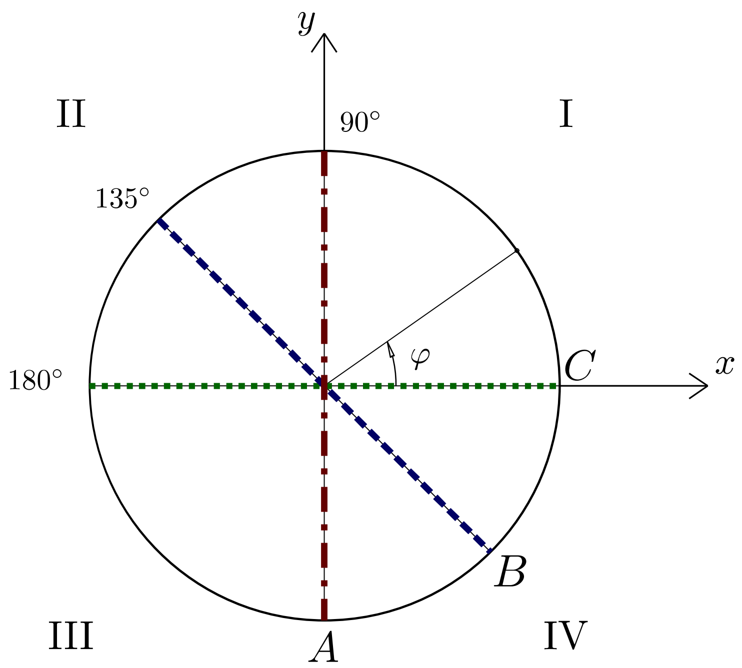

Figure 12: Upper view of the dome, where the positions of the selected meridians for the anti-symmetric load case are highlighted.

as discussed before and shape and kind of constraints do not substantially affect the stresses.

Fig. 15 (left) shows the membrane stress σ_ϑ for meridian C. Again, the effect of the load is remarkable for ϑ/ϑ_f between 0 and 1, while on the opposite side it is practically negligible except near the constraint, where stress peaks are localised. Fig. 15 (right) shows the membrane stress σ_φ for meridian C. The situation is the same as discussed before and no substantial differences can be observed between the four curves.

Fig. 16 (left) displays M_ϑ/M_0 distribution along meridian A. The pure membrane behaviour is confirmed until ϑ/ϑ_f reaches values ± 0.8. Outside this range the bending effect is relevant and peaks are localized on the con-

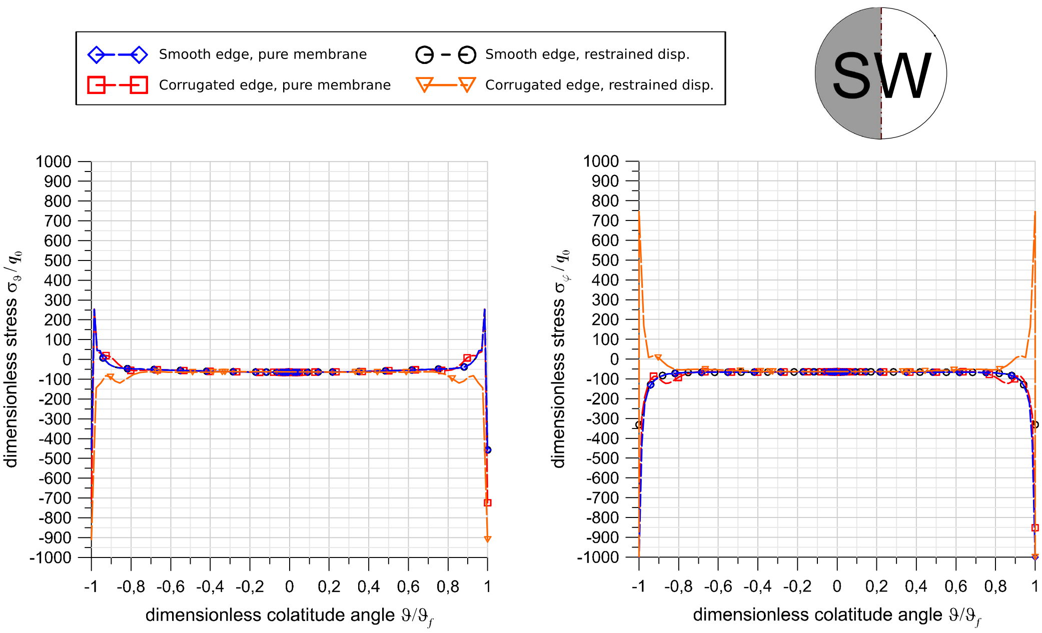

Figure 13: Anti-symmetric Load - Stress components σ_ϑ (left) and σ_φ (right) for a meridian A passing through two supports located at $\varphi = 90°$.

straints for all the four curves, especially for the corrugated-edge shell in pure membrane boundary condition. Fig. 16 (right) shows M_φ/M_0. The pure membrane behaviour stands in the range $-0.8 < \vartheta/\vartheta_f < 0.8$, then bending effects are remarkable. The effect of boundary conditions at the edge is not relevant at the edge. On the contrary, corrugation modifies considerably the moment distribution.

Fig. 17 (left) shows M_ϑ/M_0 along meridian B. The pure membrane behaviour is limited to ϑ/ϑ_f ranges of $[0.3, 0.7]$ and $[-0.7, -0.3]$. Outside these intervals the bending effect is relevant. Peaks of section moments are observed in apex because of the sudden change of load distribution. The four curves do not show significant change due to shape. Fig. 17 (right) illustrates

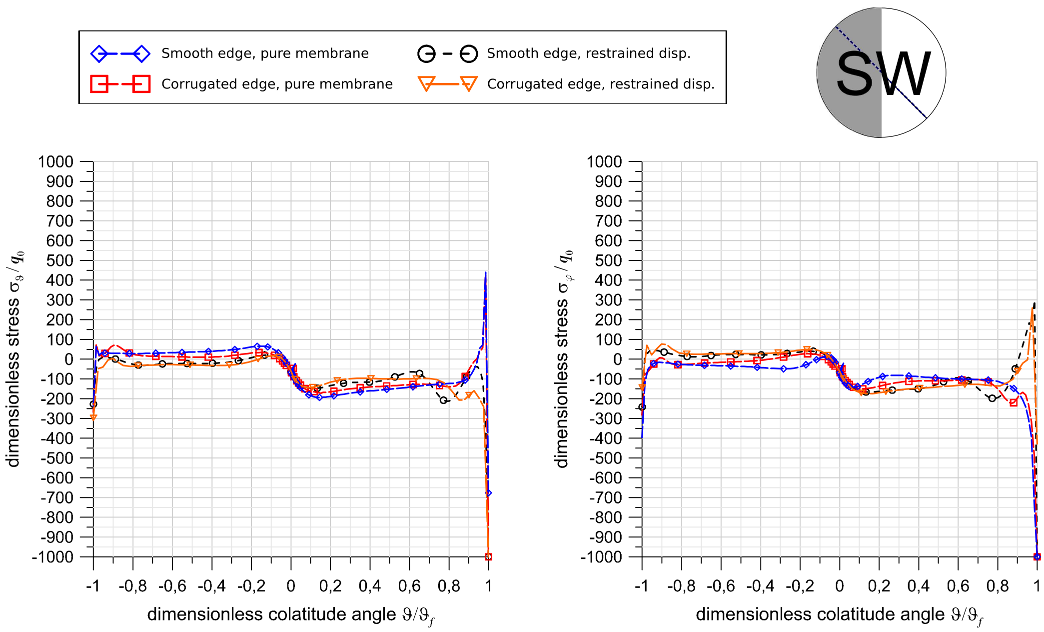

Figure 14: Anti-symmetric Load - Stress components σ_ϑ (left) and σ_φ (right) for a meridian B passing through two supports located at $\varphi = 135°$.

M_φ/M_0 distribution. Along the same meridian B the behaviour is similar to the previous, since pure membrane behaviour is enclosed in narrow intervals and bending effects are not negligible. Again, no enhancement is provided by corrugated shape.

Fig. 18 (left) shows M_ϑ/M_0 distribution. Lack of symmetry is evident and pure membrane behaviour is limited to minor part of the meridian. Mainly the bending effects are relevant, with section moment peaks located around the apex and near the edge. The corrugated edge shell shows highly localized bending moment at the edge in both boundary conditions. Finally, Fig. 18 (right) reports M_φ/M_0 distribution. Along the same meridian C the pure membrane behaviour is recognisable in a wider range of ϑ/ϑ_f, except

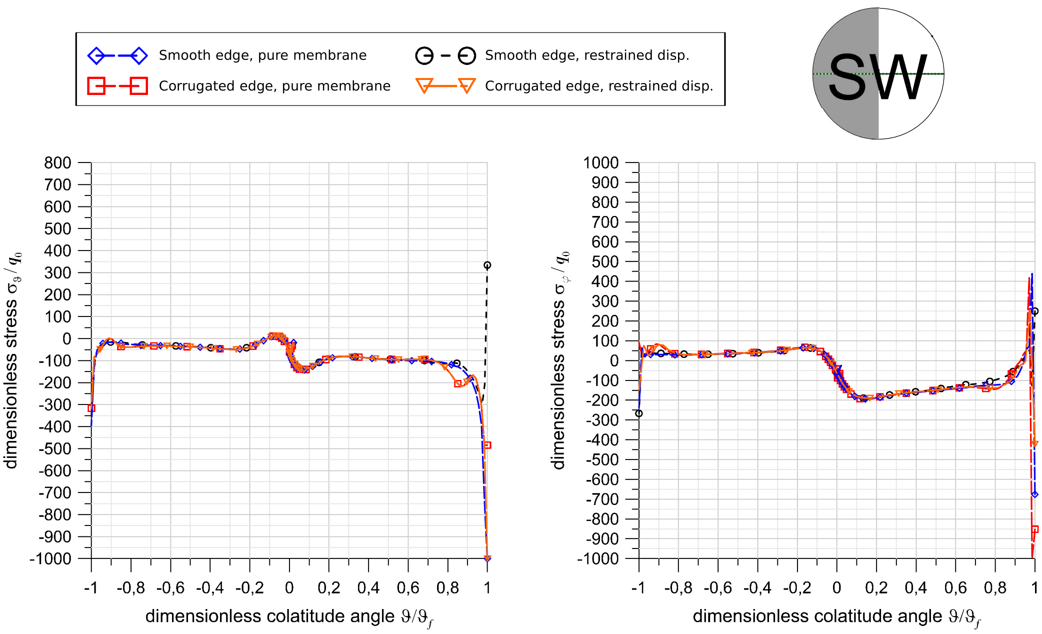

Figure 15: Anti-symmetric Load - Stress components σ_ϑ (left) and σ_φ (right) for a meridian C passing through two supports located at $\varphi = 180°$.

for the smooth edge with restrained displacements where the bending effect starts earlier. Large values of bending moment are observed at the edge, especially in the loaded part of the shell.

4. Assessment of load-bearing capacity by means of nonlinear analysis

To evaluate the influence of corrugated edge in the vertical load-bearing capacity of the dome, a non-linear static analysis has been performed. The constitutive law of the material adopted is based on the Concrete Damage Plasticity (henceforth CDP) law, that has been first developed by [34] and later improved by [35]. CDP is a plasticity and-damage-based model that

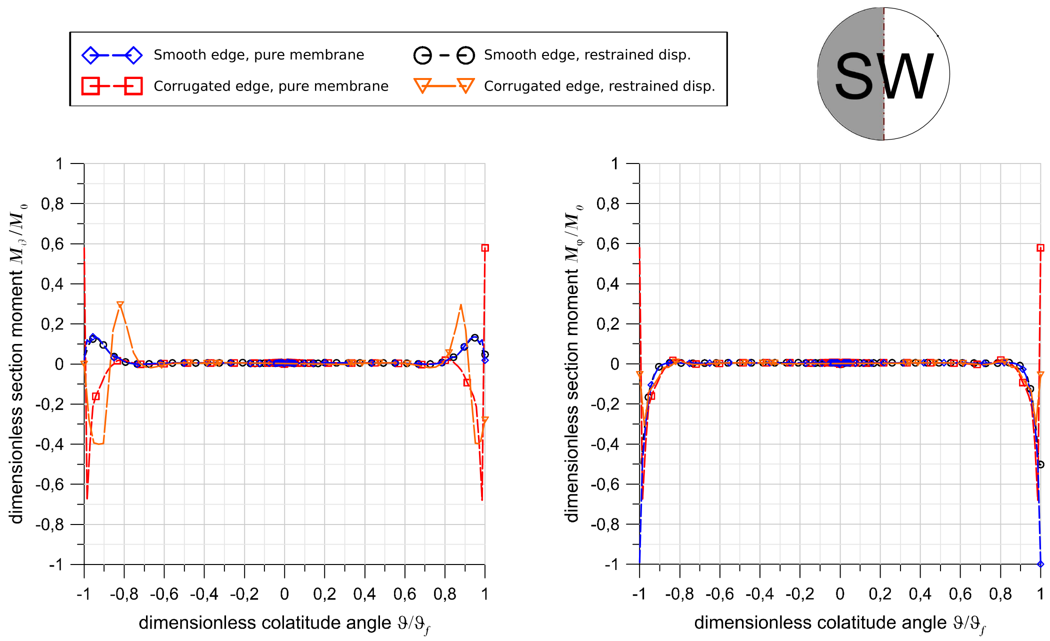

Figure 16: Anti-symmetric Load - Section moments M_ϑ (left) and M_φ (right) for a meridian A passing through two supports and located at $\varphi = 90°$.

takes into account cracking in tension and crushing in compression for defining failure mechanisms.

The model is geometrically isotropic but is able to take into consideration the tensile and compressive behaviour independently, using different parameters which regulate plasticity and damage. Fracture is implemented according to concrete-like *smeared crack* model with fixed crack orientation, that tackles Hilleborg's theory of fictitious crack [36], thus governed by a strain softening behaviour and Mode I fracture energy. The latter is intended to regularize the mesh dependency of the computational FE model due to damage and strain localization, in conjunction with the elements size, regarded as a characteristic crack band length for the material [37].

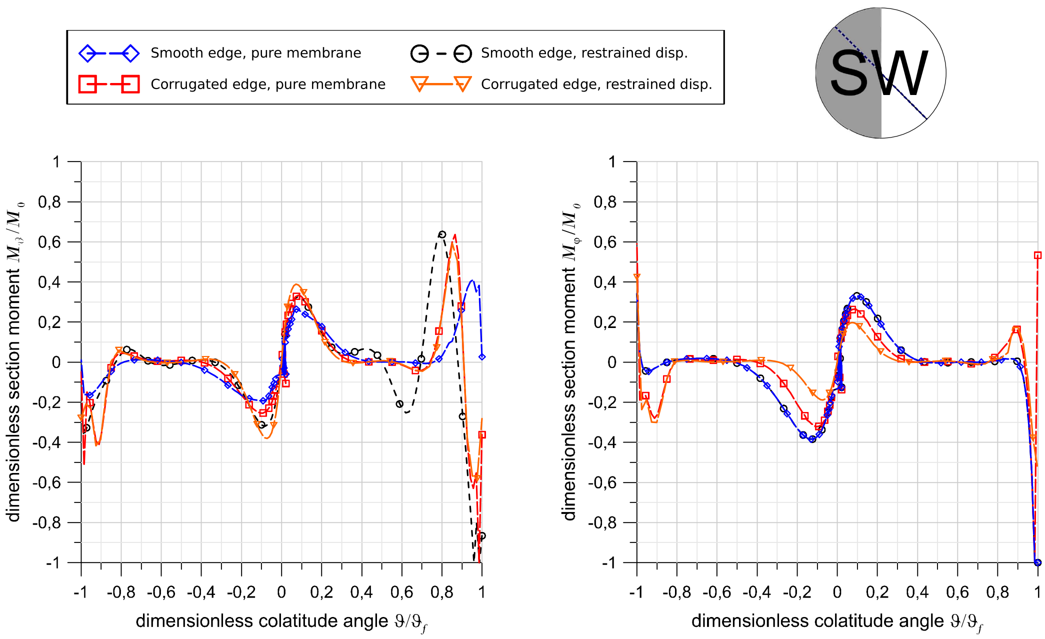

Figure 17: Anti-symmetric Load - Section moments M_ϑ (left) and M_φ (right) for meridian B, passing through two supports and located at $\varphi = 135°$.

Model parameters and adopted values are reported in Table 2. In particular: Ψ is the dilatancy angle; e ($0.1 \leq e \leq 0.3$) is the *eccentricity* that smooths the meridian section in proximity of the Drucker-Prager cone vertex to avoid convergence issues in the flow potential; f_{bo}/f_{co} is the ratio of biaxial compressive to uniaxial compressive yield stress, whose value is defined according to that suggested for concrete-like materials [34]; K_c ($0.5 \leq K_c \leq 1$) is the parameter that adapts the shape of the triaxial yield surface in such a way that in the deviatoric plane it varies from the classic Drucker-Prager circle for $K_c = 1$, to a Rankine-like triangle when lower values are assumed; ν is the viscosity parameter. The stress-strain curves for compression and tension implemented in the FE model are reported in Fig. 19, while Fig. 20

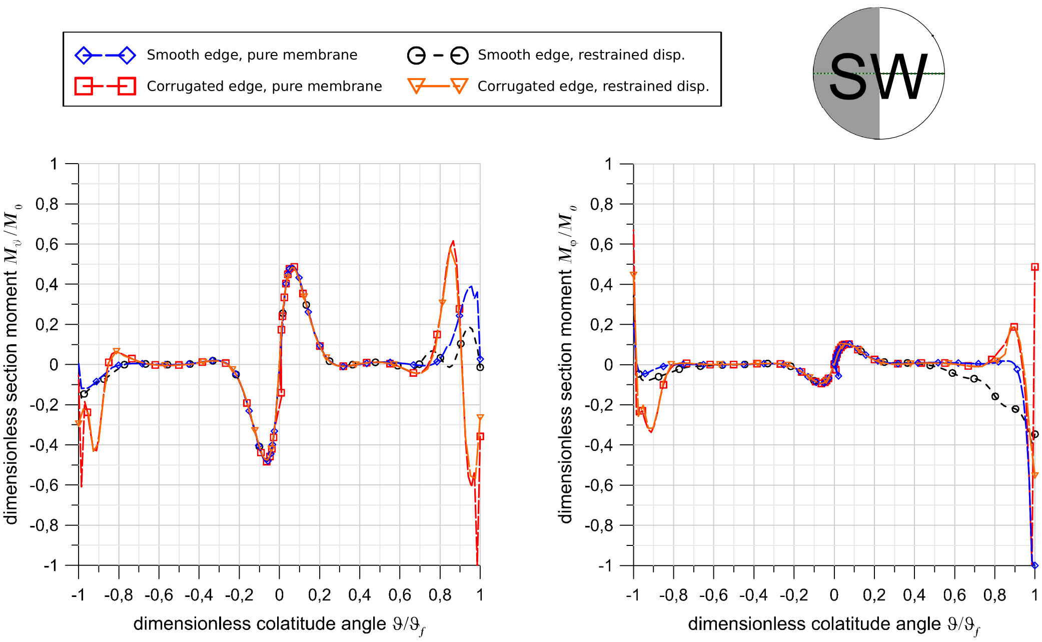

Figure 18: Anti-symmetric Load - Section moments M_ϑ (left) and M_φ (right) for meridian C, passing through two supports and located at $\varphi = 180°$.

shows the related damage curves, which describe the evolution of the damage variables in tension and compression affecting the elasticity matrix. The structure has been subjected to its self-weight q_0, regarded as the most representative load-case, then to an incremental vertical load $q = \lambda q_0$, where lambda is a load multiplier (≥ 1). The non-linear behaviour is assessed by increasing the vertical load q up to collapse. To highlight the influence of cor-

Table 2: Parameters of Concrete Damage Plasticity model

Ψ [°]	e	$\frac{f_{b0}}{f_{c0}}$	K_c	ν
35	0.10	1.16	0.667	0.007985

Table 3: q_0S and dz_0, the values for corrugated and smooth edge.

Edge shape	q_0S [kN]	dz_0 [mm]
smooth	15792.89	1.91
corrugated	15628.33	1.71

rugation, a comparison between the capacity curves obtained for the smooth and the corrugated edge shells is provided in Fig. 21. In the curves the dome apex is chosen as a control point, whose vertical displacement dz has been monitored. In the curves the displacement is normalized with respect to the initial vertical displacement dz_0 due to self-weight, as well as the vertical load q is normalized with respect to the self-weight q_0, so that the load multiplier λ is directly reported in the graph. Since smooth and corrugated edge domes have different volumes, their total weights q_0S (where S stands for shell area), along with the relative initial vertical displacements dz_0, are reported in Table 3. Due to convergence drawbacks, related to the concentration of damage at the supports the analyses stopped prematurely. Nevertheless, the subsequent considerations can be highlighted. The obtained curves show differences in terms of slope of the linear elastic branch. In fact, it is possible to notice that the corrugated edge dome exhibits a linear elastic behaviour for values of the load multiplier larger than the smooth dome, with an increase equal to about 1.6 times. This difference is due to the greater geometrical stiffness provided by the corrugation at the edge. This increase in stiffness can be also evaluated looking at the apex displacements at the end of the elastic phase: in the case of the smooth dome the apex displacement is about

1.8 times larger than that of the corrugated edge dome. Furthermore, the corrugated edge dome shows a vertical load-bearing capacity greater than the smooth edge dome. In both domes, the collapse is reached with the same mechanism, where the damaged zones are concentrated in correspondence to the supports, as reported in Fig. 22. The occurring of the same mechanism of failure, but associated to different values of load multipliers suggests that the larger geometrical stiffness due to corrugation at the edge plays an effective role also in the load bearing capacity of the dome.

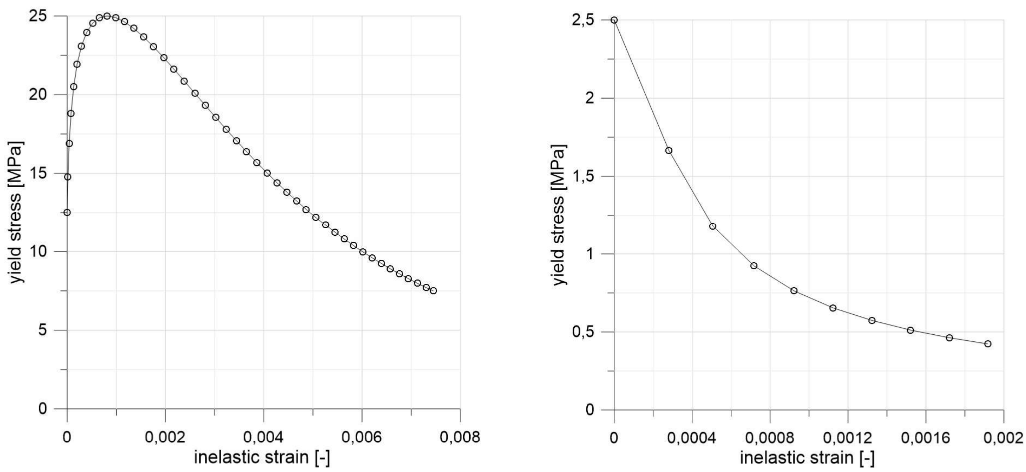

Figure 19: Stress-strain curves: compression (left) and tension (right) branches.

5. Effect of corrugation on buckling behaviour

This section deals with the assessment of the edge-corrugated shell performance in comparison with the smooth shape, with respect to instability issues. The effects of bending stiffness increment in spherical shells towards buckling has been envisaged in [38]. The presented analyses are inspired by the works [39–41]. The theoretical critical load for a complete spherical shell

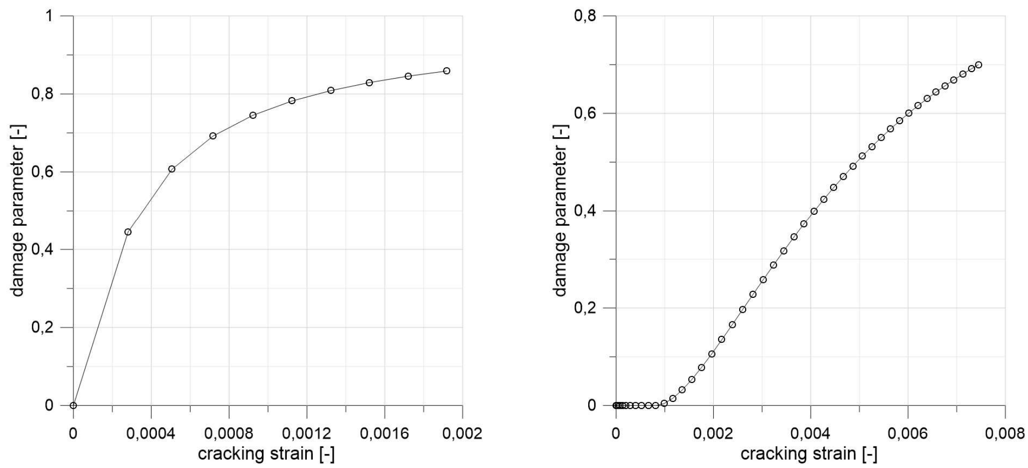

Figure 20: Damage curves: compression (left) and traction (left) branches.

has been widely treated in the scientific literature, among the several sources, [42] is selected as the preferred one.

The main problem when dealing with spherical shell instability issues is that the theoretical load is not reliable for design purposes; in fact, experimental campaigns carried out over the last century have widely proven that designers should adopt precautions against the actual ultimate load. This discrepancy is triggered essentially by geometry and material imperfections, as clearly elucidated by the eminent work of Koiter [43]. Recent studies about spherical shells buckling have been carried out making use of FE calculation, see for instance [44–46]. The American Code assessment procedure against instability is based upon [47, 48]. The method consists in employing several empirical *knock-down* factors that decrease the theoretical buckling load by globally taking into account the presence of: imperfections, creep, plasticity, cracking and, eventually, of reinforcements. To each of these effects corresponds an appropriate partial factor. This method has a major

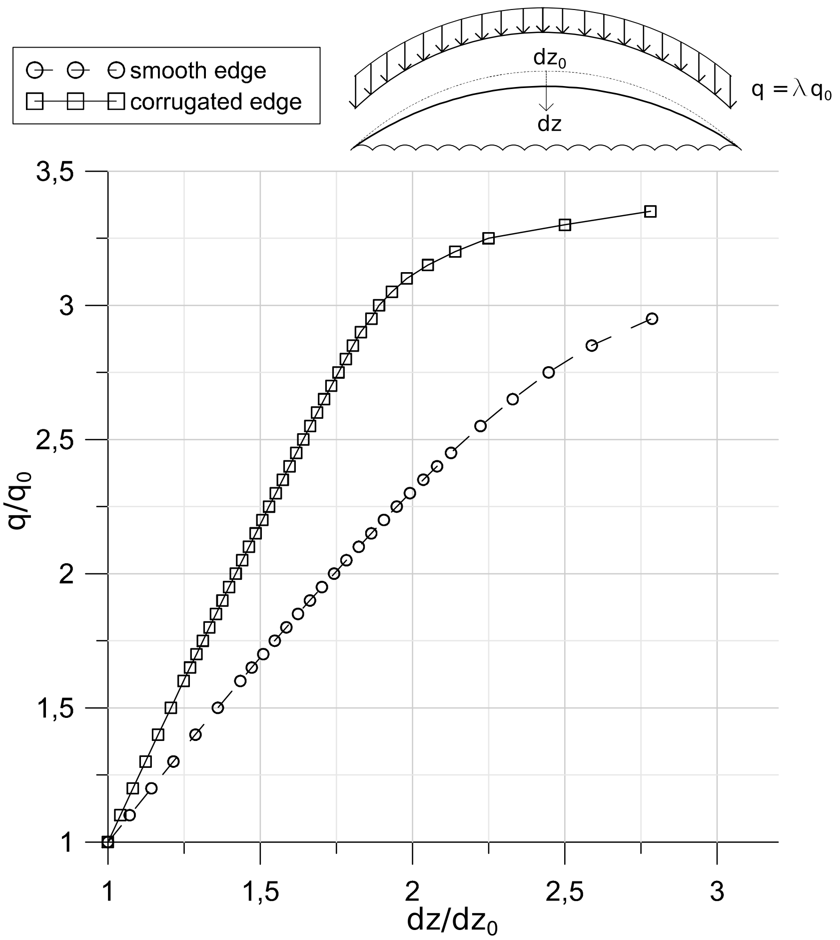

Figure 21: Capacity curve for the dome modelled with CDP.

drawback, *i.e.* it is too conservative and the ultimate load may result as low as 20 % of theoretical load, with a considerable increase of building costs. Research is ongoing on ascertaining a less conservative approach without jeopardising structural safety (see [49]). In this section, a non-linear instability analysis of the corrugated dome will be shown, taking into account only geometrical imperfections. In order to understand the effects of shell edge-corrugation towards instability, imperfections have been accounted in

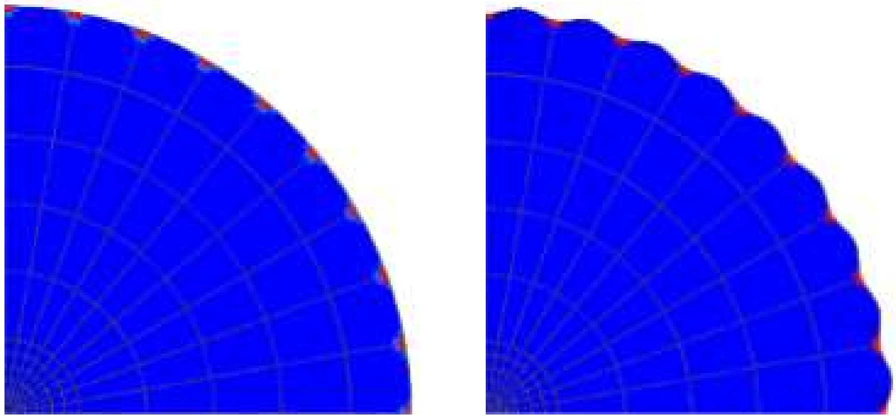

Figure 22: Damage zones highlighted for both domes (left): smooth edge (right): corrugated edge.

the form of eigen-shapes provided by a FE linear buckling analysis. The geometrical and mechanical properties used for the model are the same already employed throughout the previous Sections. This time, only the restrained displacements boundary condition has been employed at supports.

A finite strain 4-nodes shell element has been adopted for the post-buckling analysis [50], which has been carried out by means of Riks' arc-length incremental algorithm [51–53].

Hereafter, the analysed load-case is the dome self-weight, $q_0 = \gamma\, t$, where γ is the specific weight. Fig. 23 compares the first five buckling eigen-shapes for a smooth edge shallow dome (left) and for the corrugated-edge one (right). The contour plot depicts the displacement magnitude distribution upon the deformed shape. Table 4 reports the corresponding first five eigenvalues, highlighting the percentage difference in the third column. As shown, there is always an improvement in the critical load due to the edge-corrugation, which varies from 3.6% up to 6.0% for the fifth mode. It is noteworthy that the presence of the corrugation breaks the symmetry coupling of eigenvalues in the spherical case. Moreover, the increased stiffness of the corrugated edge prevents the occurrence of instability nearby the edge, which is shifted to higher modes. That is why the first three eigen-modes of the corrugated-edge shell are far different from those of the smooth one.

Fig.24 shows the outcomes of non-linear stability analyses with description of post-buckling behaviour with regards to the cases of smooth spherical dome (left) and corrugated-edge dome (right) for perfect ideal shapes (black line) and imperfect real shapes (blue line). The presented curves are the equilibrium path identified by means of an arc-length incremental procedure in large displacements. Geometrical imperfections have been modelled for both shells according to the respective first buckling mode-shapes scaled by a factor of 0.1 and assumed as the undeformed initial geometry. As anticipated, y-axis reports the load-multiplier applied to the structure self-weight. Regarding the smooth shell case on the left, the description of the ideal case, *i.e.* with no imperfections, has encountered irrecoverable convergence issues, probably due to the presence of a bifurcation equilibrium point, therefore no critical load and no post-buckling mode have been evaluated. On the other hand, the case of geometrically *imperfect* shell has been completely exploited and both the buckling load and the post-buckling behaviour have been clearly determined, the latter showing a snap-through response. Hence, it is still possible to argue that the buckling load has consistently decreased due to the imperfection introduced in the model with respect to the perfect case and further reduction is to be expected if the imperfection scaling factor is amplified. Analogous comments can be outlined for the case of

Table 4: Eigenvalues of the linear buckling analysis

	smooth	corrugated	difference [%]
1^{st}	99.804	104.66	3.6 %
2^{nd}	99.804	104.67	3.7 %
3^{rd}	99.923	104.81	3.9 %
4^{th}	99.923	106.52	5.6 %
5^{th}	99.994	106.93	6.0 %

the corrugated-edge shell, which has been completely developed both in the case of perfect geometry and of imperfect geometry. Hence, it is possible to evaluate the effect of such an imperfection, in terms of a knock-down factor of about 0.60 on the critical load, but, even for the ideal case, it has been possible to point out a remarkable critical load reduction, about 35%, with respect to the first eigen-value determined via the linear procedure. Since the presented cases are based on geometrical imperfections modelled on the respective the first buckling mode-shapes, in this section no meaningful comparison is possible between smooth and corrugated-edge shells behaviours.

6. Conclusion

This paper addresses the effects of an edge shape modification on the structural behaviour of shallow spherical shells under discrete support boundary conditions. In particular, the introduced geometrical perturbation consists of a wavy co-sinusoidal corrugation applied nearby the supported boundary, whose mathematical representation is given in Sec 2. The structural behaviour modification and possible improvement caused by this geometrical perturbation have been evaluated from different points of view and concerning several load scenarios and boundary conditions. Numerical analyses presented here support Nervi's insight of Flaminio stadium reinforced concrete rooftop.

In Section 3 the linear elastic structural behaviour has been analysed with respect to several typical load-cases under pure membrane and displacements restrained boundary conditions. The comparison between the spherical and the corrugated dome reports of a prevalent improvement for the pressure load case and a less significative one for the self-weight load. On the whole, the section moments for the corrugated shape denote a moderate reduction. In the case of anti-symmetrical distributed load no major improvements are observed, apart from a slight decrease in the stresses at supports. Ultimate load bearing capacity has been compared in Section 4, taking into account plasticity of reinforced concrete. This time the enhancement of the structural performance has been clearly disclosed in terms of stiffness and collapse load. Section 5 deals with the influence of the shape corrugation on buckling behaviour in linear and non-linear fields. Given the relevance of this problem in thin-shell structures, the buckling behaviour will be studied more comprehensively in a forthcoming paper, to ascertain how the discussed geometry affects the stability of such shells and to discuss a prospective corrugation optimisation.

7. Declaration of competing interest

The authors declare that they have no known competing financial interests or personal relationships that could have appeared to influence the work reported in this paper.

8. Acknowledgements

This research has been developed for the partial fulfillment of the doctoral program of M. Lai at *Scuola di dottorato in Ingegneria Civile e Architettura, University of Cagliari*.

The financial support of Fondazione di Sardegna through grant *Surveying, modelling, monitoring and rehabilitation of masonry vaults and domes* i.e. *Rilievo, modellazione, monitoraggio e risanamento di volte e cupole in muratura (RMMR)* (CUP code: F72F20000320007) is grateful acknowledged by M. Lai, E. Reccia, A. Cazzani.

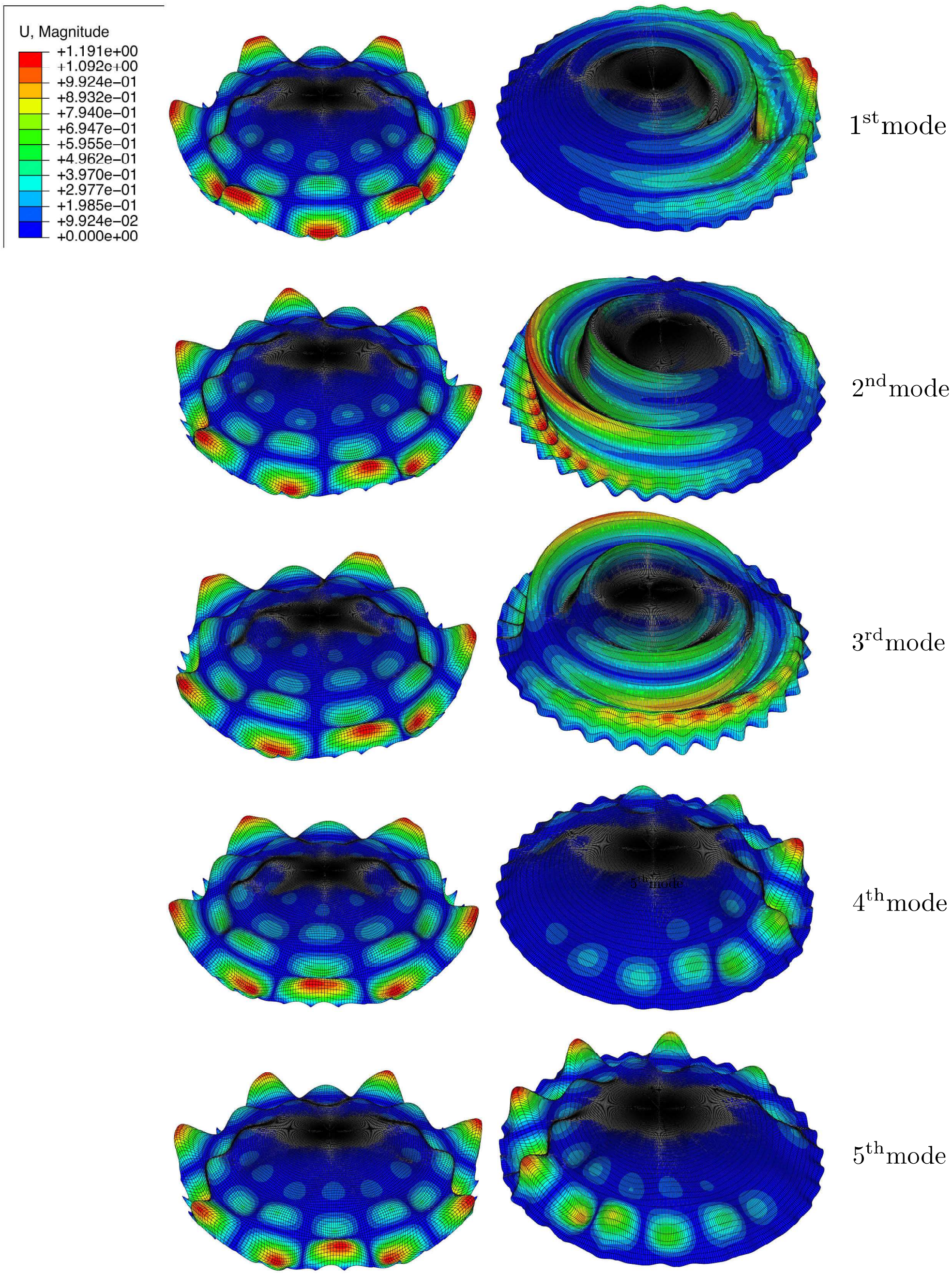

Figure 23: Comparison of the eigenshapes; (left) shapes for the smooth dome (right), shapes for the edge-corrugated dome.

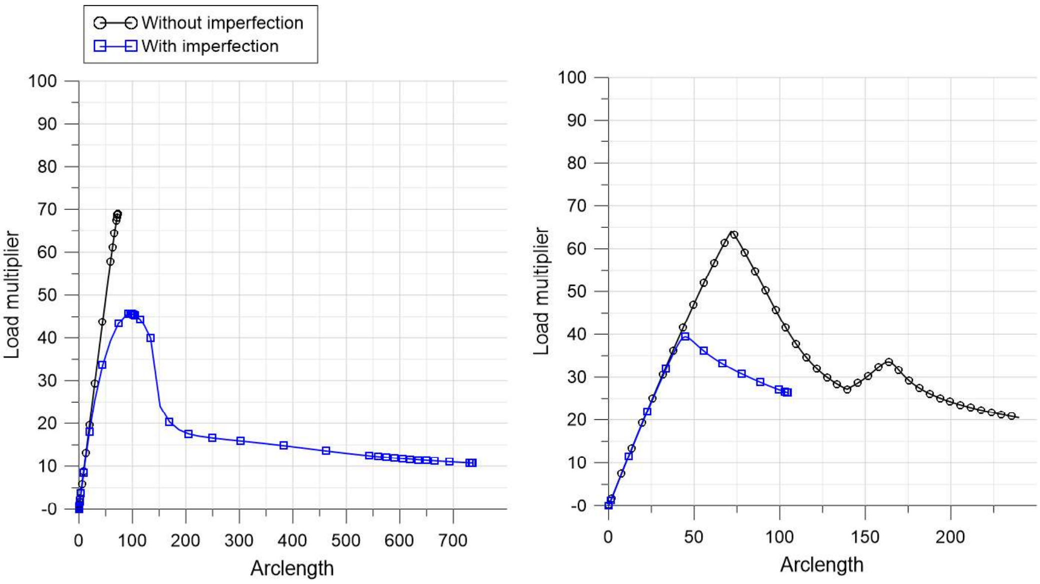

Figure 24: Equilibrium paths: (left) smooth dome; (right) edge-corrugated dome.

References

[1] A. E. H. Love, *A treatise on the mathematical theory of elasticity*. Cambridge: Cambridge university press, 1893.

[2] W. Flügge, *Stresses in shells*. Berlin: Springer, 1960.

[3] C. Siegel, *Structure and form in modern architecture*. New York: Reinhold, 1966.

[4] G. Pizzetti and A. M. Zorno Trisciuoglio, *Principi statici e forme strutturali*. Torino: Utet, 1980.

[5] J. Geckeler, *Über die Festigkeit achsensymmetrischer Schalen, Forschungsarbeiten auf dem Gebiet des Ingenieurwesens*. Berlin: VDI-Verlag, 1926.

[6] M. Hetényi, "Spherical shells subjected to axial symmetrical bending", *Publications International Association for Bridge and Structural Engineering, (IABSE) Bulletin*, vol. 5, pp. 173–185, 1938.

[7] P. L. Nervi, G. Neri, M. A. Chiorino, and A. Rossi, *Scienza o arte del costruire?: Caratteristiche e possibilità del cemento armato*. Milano: CittàStudi, 2014.

[8] P. L. Nervi, *Costruire correttamente*. Roma: Hoepli, 1955.

[9] T. Leslie, "Carpenter's parametrics: economics, efficiency, and form in Pier Luigi Nervi's concrete designs", *Journal of the International Association for Shell and Spatial Structures*, vol. 54, pp. 107–115, 2013.

[10] T. Iori and S. Poretti, eds., *SIXXI. Storia dell'ingegneria strutturale in Italia*, vol. 1-5. Roma: Gangemi, 2014.

[11] T. Iori and R. Sulpizio, "La cupola del Palazzetto di Pier Luigi Nervi", *Industria Italiana del Cemento*, no. 857, pp. 16–23, 2022.

[12] A. M. Haas, *Thin concrete shells*, vol. 2. New York: Wiley, 1967.

[13] S. P. Timoshenko and S. Woinowsky-Krieger, *Theory of plates and shells*. New York: McGraw-Hill, 2nd ed., 1959.

[14] V. V. Novozhilov, *Thin shell theory*. Groningen: Wolters–Noordhoff, 2nd ed., 1970.

[15] V. G. Rekach, *Static theory of thin-walled space structures*. Moscow: Mir, 1978.

[16] A. M. Haas, *Thin concrete shells*, vol. 1. New York: Wiley, 1962.

[17] D. P. Billington, *Thin shell concrete structures*. New York: McGraw-Hill, 1965.

[18] V. Gioncu, *Thin reinforced concrete shells: special analysis problems*. Bucarest: Wiley, 1979.

[19] S. J. Medwadowski and E. P. Popov, eds., *Concrete shell buckling*. Cambridge (Ma): American Concrete Institute, 1981.

[20] CEN, ed., *EN1993-4-2. Eurocode 3 - Design of steel structures - Part 1-6: Strength and Stability of Shell Structures*. 2007.

[21] F. Leonhardt and E. Mönnig, *C.a. &c. a.p.: calcolo di progetto & tecniche costruttive*. 1979.

[22] P. G. Gambarova, D. Coronelli, and P. Bamonte, *Linee guida per la progettazione di piastra in c.a.* Bologna: Patron, 2007.

[23] G. M. Calvi and R. Nascimbene, *Progettare i gusci*. Pavia: IUSS Press, 2011.

[24] T. Michiels, S. Adriaenssens, and M. Dejong, "Form finding of corrugated shell structures for seismic design and validation using non-linear pushover analysis", *Engineering Structures*, vol. 181, pp. 362–373, 2019.

[25] C. Olivieri, M. Angelillo, A. Gesualdo, A. Iannuzzo, and A. Fortunato, "Parametric design of purely compressed shells", *Mechanics of Materials*, vol. 155, p. 103782, 2021.

[26] J. M. Rotter, G. Mackenzie, and M. Lee, "Spherical dome buckling with edge ring support", *Structures*, vol. 8, pp. 264–274, 2016.

[27] A. Zingoni, "Stress and buckling resistance of dual-purpose concrete shells", *Thin-Walled Structures*, vol. 170, p. 108596, 2022.

[28] Z. Chang, M. A. Bradford, and R. I. Gilbert, "Limit analysis of local failure in shallow spherical concrete caps subjected to uniform radial pressure", *Thin-Walled Structures*, vol. 48, pp. 373–378, 2010.

[29] M. Lai, S. R. Eugster, E. Reccia, M. Spagnuolo, and A. Cazzani, "Corrugated shells: An algorithm for generating double-curvature geomet-

ric surfaces for structural analysis", *Thin-Walled Structures*, vol. 173, p. 109019, 2022.

[30] P. Solomita, *Pier Luigi Nervi vaulted architecture: towards new structures*. Bologna: Bononia University Press, 2015.

[31] T. Iorio and S. Poretti, "Pier Luigi Nervi: His construction system for shell and spatial structures", *Journal of the International Association for Shell and Spatial Structures*, vol. 54, no. 2–3, pp. 117–126, 2013.

[32] I. Bucur-Horváth and R. V. Săplăcan, "Force lines embodied in the building: Palazzetto dello sport", *Journal of the International Association for Shell and Spatial Structures*, vol. 54, no. 2-3, pp. 179–187, 2013.

[33] W. Miroslaw, "Concept of shell-beam model of slab-column connection based on analysis of the 3d model", *Procedia Engineering*, vol. 65, pp. 158–165, 2013.

[34] J. Lubliner, J. Oliver, S. Oller, and E. Oñate, "A plastic-damage model for concrete", *International Journal of Solids and Structures*, vol. 25, pp. 299–326, 1989.

[35] J. Lee and G. L. Fenves, "Plastic-damage model for cyclic loading of concrete structures", *ASCE Journal of Engineering Mechanics*, vol. 124, no. 8, pp. 892–900, 1998.

[36] A. Hillerborg, M. Modéer, and P. E. Petersson, "Analysis of crack formation and crack growth in concrete by means of fracture mechanics and finite elements", *Cement and concrete research*, vol. 6, pp. 773–781, 1976.

[37] Z. P. Bažant and J. Planas, *Fracture and size effect in concrete and other quasibrittle materials*. Boca Raton: Routledge, 2019.

[38] T. von Kármán and H.-S. Tsien, "The Buckling of spherical shells by external pressure", *Journal of the Aeronautical Sciences*, vol. 7, pp. 43–50, 1939.

[39] M. Pignataro, N. L. Rizzi, and A. Luongo, *Stability, bifurcation, and postcritical behaviour of elastic structures*. Amsterdam: Elsevier, 1991.

[40] N. L. Rizzi and V. Varano, "The effects of warping on the postbuckling behaviour of thin-walled structures", *Thin-Walled Structures*, vol. 49, pp. 1091–1097, 2011.

[41] N. L. Rizzi, V. Varano, and S. Gabriele, "Initial postbuckling behavior of thin-walled frames under mode interaction", *Thin-Walled Structures*, vol. 68, pp. 124–134, 2013.

[42] W. T. Koiter and A. M. A. van der Heijden, *W. T. Koiter's elastic stability of solids and structures*. Cambdridge: Cambridge University Press, 2009.

[43] W. T. Koiter, "On the nonlinear theory of thin elastic shells", *Proc. Koninkl. Ned. Akad. van Wetenschappen, Series B*, vol. 69, pp. 1–54, 1966.

[44] H. Wagner, C. Hühne, and S. Niemann, "Robust knockdown factors for the design of spherical shells under external pressure: Development and validation", *International Journal of Mechanical Sciences*, vol. 141, pp. 58–77, 2018.

[45] H. Wagner, C. Hühne, J. Zhang, W. Tang, and R. Khakimova, "Geometric imperfection and lower-bound analysis of spherical shells under external pressure", *Thin-Walled Structures*, vol. 143, p. 106195, 2019.

[46] H. Wagner, C. Hühne, J. Zhang, and W. Tang, "On the imperfection sensitivity and design of spherical domes under external pressure", *International Journal of Pressure Vessels and Piping*, vol. 179, p. 104015, 2020.

[47] S. J. Medwadowski, ed., *Recommendations for reinforced concrete shells and folded plates*. IASS, 1979.

[48] E. Dulácska and L. Kollár, "Design procedure for the buckling analysis of reinforced concrete shells", *Thin-Walled Structures*, vol. 23, no. 1, pp. 313–321, 1995.

[49] F. L. Jiménez, J. Marthelot, A. Lee, J. W. Hutchinson, and P. M. Reis, "Technical brief: Knockdown factor for the buckling of spherical shells containing large-amplitude geometric defects", *Journal of Applied Mechanics*, vol. 84, no. 3, 2017.

[50] B. Budiansky, "On the'best' first-order linear shell theory", *The Prager Anniversary Volume–Progress in Applied Mechanics*, 1963.

[51] E. Riks, "The application of Newton's method to the problem of elastic stability", *Journal of Applied Mechanics*, vol. 39, no. 4, pp. 1060–1065, 1972.

[52] E. Riks, "An incremental approach to the solution of snapping and buckling problems", *International Journal of Solids and Structures*, vol. 15, no. 7, pp. 529–551, 1979.

[53] M. Crisfield, "A fast incremental/iterative solution procedure that handles "snap-through"", *Computers & Structures*, vol. 13, no. 1, pp. 55–62, 1981.

Declaration of interests

☒ The authors declare that they have no known competing financial interests or personal relationships that could have appeared to influence the work reported in this paper.

☒The authors declare the following financial interests/personal relationships which may be considered as potential competing interests:

This research has been developed for the partial fulfillment of the doctoral program of M. Lai at Scuola di dottorato in Ingegneria Civile e Architettura, University of Cagliari.
The financial support of Fondazione di Sardegna through grant Surveying, modelling, monitoring and rehabilitation of masonry vaults and domes i.e. Rilievo, modellazione, monitoraggio e risanamento di volte e cupole in muratura (RMMR) (CUP code: F72F20000320007) is grateful acknowledged by M. Lai, E. Reccia, A. Cazzani.